20. Remote Sensing of the Spheres

Stefan Wunderle, Mathias Kneubühler, Dominik Brunner, Alain Geiger

Swiss Commission for Remote Sensing,
Swiss Geodetic Commission

TALKS:

20.1 *Ahmed K.R., Paul-Limoges E., Rascher U., Damm A.*: Impact of the 2018 European drought on ecosystem evapotranspiration: A remote sensing perspective

20.2 *Augustin H., Sudmanns M., Tiede D., Weber H., Neuhaus C., Wunderle S., Hummer P., Reichel S., van der Meer L., Baraldi A.*: SemantiX: a cross-sensor semantic EO data cube to open and leverage AVHRR time-series and essential climate variables with scientists and the public

20.3 *Eruteya O.E., Niyazi Y., Omosanya K.O., Ierodiaconou D., Moscariello A.*: Morphology of rafted blocks in a buried landslide: A case study from the Exmouth Plateau, offshore NW Australia

20.4 *Frey O., Werner C.L., Manconi A., Coscione R.*: Measing surface displacements using a novel UAV/car-borne radar interferometer: including a case study on a fast-moving landslide in Brinzauls

20.5 *Gupana R., Odermatt D., Damm-Reiser A.*: Remote sensing of sun-induced fluorescence in inland and coastal waters: current state and future prospects

20.6 *Hadjipetrou S., Kyriakidis P., Mariethoz G.*: Geostatistical downscaling of offshore coarse spatial resolution wind speed data using satellite-derived wind information

20.7 *Hohensinn R., Rothacher M.*: How small can ground movements be in order to be detected with GNSS?

20.8 *Kellenberger B., Veen T., Folmer E., Tuia D.*: Efficient high-density bird colony censuses using drones and convolutional neural networks

20.9 *Manconi A., Caduff R., Strozzi T., Frey O., Werner C., Wegmuller U.*: Monitoring displacements of complex landslide scenarios with broadband multiplatform radar techniques

20.10 *Moeller G., Ao C.O.*: Atmospheric tomography – a valuable asset for future CubeSat missions

20.11 *Müller L., Chen K., Rothacher M.*: Refinement of CubeSat orbit determination using on-board velocity solutions

20.12 *Odermatt D., Runnalls J., Sturm J., Damm A.*: SenCast: Instant Copernicus satellite data and analysis

20.13 *Petibon F., Czyz E., Ghielmetti G.,* Hueni H., Kneubühler M., Schaepman M.E. , Schuman M.C.: Typical Uncertainties in Measurements of Leaf Optical Properties Still Permit Detection of Fine-Scale Biological Variation

20.14 *Sauvageat E., Hagen J., Kotiranta M., Hocke K., Gomez M., Neduloha G., Murk A.*: Comparison of three high resolution real-time spectrometers for microwave ozone profiling instruments

20.15 *Shehaj E., Moeller G., Geiger A., Frey O., Rothacher M.*: Mapping 3D tropospheric variables in an Alpine Region by collocation of tropospheric delays in spaceborne microwave signals

20.16 *Sturm J., Damm A.*: Drought-induced Impacts on Forest Health in Switzerland: A Remote Sensing Perspective

POSTERS:

P 20.1 *Prakash N., Manconi A., Loew S.*: Mapping Event Landslides from Satellite Images Using Convolutional Neural Networks

P 20.2 *Jing Xie*: Both urbanization and elevation constrict forest greening in the Pearl River Delta, China

20.1
Impact of the 2018 European drought on ecosystem evapotranspiration: A remote sensing perspective

Kazi Rifat Ahmed[1], Eugénie Paul-Limoges[1], Uwe Rascher[2] & Alexander Damm[1,3]

[1] Department of Geography, University of Zurich, Zurich, Switzerland
[2] Plant Science (IBG-2), Institute of Bio- and Geosciences, Forschungszentrum Jülich, Germany
[3] Swiss Federal Institute of Aquatic Science and Technology, Surface Waters – Research and Management, Dübendorf, Switzerland

The combined drought and heat-wave affecting Europe in 2018 was one of the most extreme events in the last decades. Recent studies already assessed and confirmed the severity of this extreme event on ecosystems using greenness proxies with remote sensing data (Buras et al., 2020; Schuldt et al., 2020). Droughts and heat-waves compose a complex set of abiotic driver that determine ecosystem water fluxes, i.e., evapotranspiration (ET), by affecting plant water availability (e.g., soil moisture) and atmospheric water demand (e.g., vapor pressure deficit, relative humidity, air temperature) (Orth and Destouni, 2018; Sippel et al., 2018). Assessing ET, therefore, provides an additional strategy to evaluate the impact of droughts and heat-waves on ecosystem integrity via a complementary functional perspective. Besides, ET is considered an essential environmental process to determine the state of ecosystem functioning in response to extreme climate events (Bonan, 2008; Lawrence et al., 2007). Recent studies demonstrated, for example, the feasibility of ET to study the impact of droughts on ecosystem water deficit (Dang et al., 2019; Hanel et al., 2018; Orth and Destouni, 2018; Sippel et al., 2018; Teuling, 2018).

In this study, we aim to evaluate the effect of the combined drought and heat-wave in 2018 on ET across European ecosystems and to unravel causality to underlying abiotic drivers. We used the established and globally available 8-day ET composite obtained from the MODerate Resolution Imaging Spectroradiometer (MODIS) and investigated monthly ET anomalies in 2018 compared to a monthly reference period from 2007-2017. The MODIS ET product is based on the Penman-Monteith (PM) equation (Monteith, 1965; Penman, 1948, Mu et al., 2009), one of the most frequently used mechanistic frameworks to model ET across ecosystems. PM based ET estimates are particularly suited for our analysis since considering atmospheric and energy constraints and the biological control (e.g., canopy resistance) on ET fluxes (Allen, 2005; Langensiepen et al., 2009; Mu et al., 2011, 2007; Schymanski and Or, 2016). We additionally investigated three meteorological variables to understand causality ecosystem responses to extreme events, particularly subsurface soil moisture (NASA-USDA SMAP Global Soil Moisture Data (NASA GSFC, 2020)), total precipitation and air temperature (both from the European Centre for Medium-Range Weather Forecasts (ECMWF) (C3S, 2018)).

Our results revealed that ET in specific regions across Europe was reduced by up to 70% during the peak of the extreme event. Particularly agricultural areas (mean reduction of 15% to 20% from April to October) and non-irrigated arable land (mean reduction of 16% to 24% from April to October) in Northern Europe where affected, while forest ecosystems in Southern Europe were almost unaffected. We confronted calculated ET anomalies against anomalies of abiotic drivers (temperature, total precipitation, soil moisture) and found that particularly ecosystems with soil moisture and precipitation as dominant abiotic drivers showed the largest reductions in ET compared to ecosystems dominated by the air temperature. Our results give a first comprehensive insight into the 2018 European drought impact on ecosystem ET. Ideas on the interdependency between ecosystem functioning and driver dynamics will advance understanding of ecosystem responses and integrity and can become essential to improve ecosystem management for future environmental change.

REFERENCES

Allen, R. 2005: PENMAN – MONTEITH EQUATION. Encycl. Soils Environ. 180–188.

Bonan, G.B. 2008: Forests and climate change: Forcings, feedbacks, and the climate benefits of forests. Science (80-.). 320, 1444–1449. https://doi.org/10.1126/science.1155121

Buras, A., Rammig, A. S. & Zang, C. 2020: Quantifying impacts of the 2018 drought on European ecosystems in comparison to 2003. Biogeosciences 17, 1655–1672. https://doi.org/10.5194/bg-17-1655-2020

Copernicus Climate Change Service (C3S) (2018): ERA5 hourly data on single levels from 1979 to present. Fifth generation of ECMWF atmospheric reanalyses of the global climate. Copernicus Climate Change Service Climate Data Store (CDS). DOI: 10.24381/cds.adbb2d47. https://cds.climate.copernicus.eu/cdsapp#!/dataset/reanalysisera5-single-levels?tab=overview

Dang, H., Lu, P., Yang, W., Han, H. & Zhang, J. 2019: Drought-Induced Reductions and Limited Recovery in the Radial Growth , Transpiration , and Canopy Stomatal Conductance of Mongolian Scots Pine (Pinus sylvestris var . mongolica Litv): A Five-Year Observation.

Hanel, M., Rakovec, O., Markonis, Y., Máca, P., Samaniego, L., Kyselý, J. & Kumar, R. 2018: Revisiting the recent European droughts from a long-term perspective. Sci. Rep. 8, 1–11. https://doi.org/10.1038/s41598-018-27464-4

Langensiepen, M., Fuchs, M., Bergamaschi, H., Moreshet, S., Cohen, Y., Wolff, P., Jutzi, S.C., Cohen, S., Rosa, L.M.G., Li, Y. & Fricke, T. 2009: Quantifying the uncertainties of transpiration calculations with the Penman-Monteith equation under different climate and optimum water supply conditions. Agric. For. Meteorol. 149, 1063–1072. https://doi.org/10.1016/j.agrformet.2009.01.001

Lawrence, D.M., Thornton, P.E., Oleson, K.W. & Bonan, G.B. 2007: The partitioning of evapotranspiration into transpiration, soil evaporation, and canopy evaporation in a GCM: Impacts on land-atmosphere interaction. J. Hydrometeorol. 8, 862–880. https://doi.org/10.1175/JHM596.1

Monteith, J.L. 1965: Evaporation and environment. Symp. Soc. Exp. Biol.

Mu, Q., Heinsch, F.A., Zhao, M. & Running, S.W. 2007: Development of a global evapotranspiration algorithm based on MODIS and global meteorology data. Remote Sens. Environ. 111, 519–536. https://doi.org/10.1016/j.rse.2007.04.015

Mu, Q., Zhao, M. & Running, S.W. 2011: Improvements to a MODIS global terrestrial evapotranspiration algorithm. Remote Sens. Environ. 115, 1781–1800. https://doi.org/10.1016/j.rse.2011.02.019

NASA GSFC, 2020: NASA-USDA SMAP Global Soil Moisture Data. https://gimms.gsfc.nasa.gov/SMOS/SMAP/

Orth, R., & Destouni, G. 2018: Drought reduces blue-water fluxes more strongly than green-water fluxes in Europe. Nat. Commun. 9. https://doi.org/10.1038/s41467-018-06013-7

Penman, H.L. 1948: Natural evaporation from open water, hare soil and grass. Proc. R. Soc. Lond. A. Math. Phys. Sci. 193, 120–145. https://doi.org/10.1098/rspa.1948.0037

Schuldt, B., Buras, A., Arend, M., Vitasse, Y., Beierkuhnlein, C., Damm, A., Gharun, M., Grams, T.E.E., Hauck, M., Hajek, P., Hartmann, H., Hilbrunner, E., Hoch, G., Holloway-Phillips, M., Körner, C., Larysch, E., Lübbe, T., Nelson, D.B., Rammig, A., Rigling, A., Rose, L., Ruehr, N.K., Schumann, K., Weiser, F., Werner, C., Wohlgemuth, T., Zang, C.S. & Kahmen, A. 2020: A first assessment of the impact of the extreme 2018 summer drought on Central European forests. Basic Appl. Ecol. https://doi.org/10.1016/j.baae.2020.04.003

Schymanski, S.J., & Or, D. 2016. Wind increases leaf water use efficiency. Plant Cell Environ. 39, 1448–1459. https://doi.org/10.1111/pce.12700

Sippel, S., Reichstein, M., Ma, X., Mahecha, M.D., Lange, H., Flach, M. & Frank, D. 2018: Drought, Heat, and the Carbon Cycle: a Review. Curr. Clim. Chang. Reports 4, 266–286. https://doi.org/10.1007/s40641-018-0103-4

Teuling, A.J. 2018: A hot future for European droughts. Nat. Clim. Chang. 8, 364–365. https://doi.org/10.1038/s41558-018-0154-5

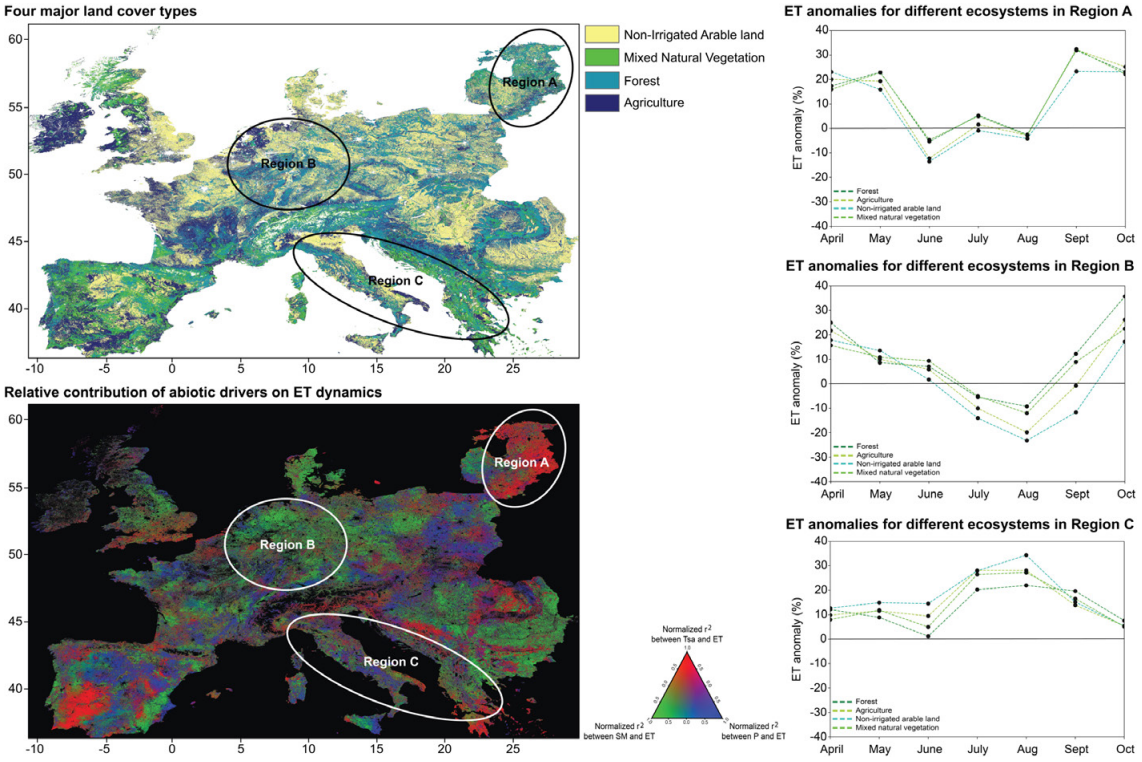

Figure 1. The graphical abstract of the study. The upper left image showing the four major land cover types. The lower left image showing the relative contribution of abiotic drivers (air temperature, precipitation, and subsurface soil moisture) on ET dynamics. The images on the right side showing the anomalies of ET for Region A, B, and C, accordingly.

20.2
SemantiX: a cross-sensor semantic EO data cube to open and leverage AVHRR time-series and essential climate variables with scientists and the public

Hannah Augustin[1], Martin Sudmanns[1], Dirk Tiede[1], Helga Weber[2], Christoph Neuhaus[2], Stefan Wunderle[2], Philipp Hummer[3], Steffen Reichel[4], Luuk van der Meer[1], & Andrea Baraldi[5]

[1] Department of Geoinformatics – Z_GIS, University of Salzburg, Schillerstrasse 30, A-5020 Salzburg (hannah.augustin@sbg.ac.at)
[2] Oeschger Center for Climate Change Research and Institute of Geography, University of Bern, Hallerstrasse 12, CH-3012 Bern
[3] SPOTTERON GMBH, Fasszieh ergasse 5/16, A-1070 Vienna
[4] Spatial Services GmbH, Schillerstrasse 30, A-5020 Salzburg
[5] Italian Space Agency, Via del Politecnico, I-00155 Rome

Long time series of essential climate variables (ECVs) derived from satellite data are key to climate research. ECVs comprise a representative set of physical, chemical, or biological variables or a group of linked variables that critically contribute to the characterisation of Earth's climate system's state, interactions and developments (Bojinski et al. 2014). They are a critical, independent source of information to compare with climate model results and can also be used to directly detect and monitor changes in our environment. One of the longest European time series (1981-now) of Advanced Very High Resolution Radiometer (AVHRR) imagery will be compiled and archived by the Remote Sensing Research Group at University of Bern. Until now, AVHRR imagery has only been accessible via sequential access, requiring a significant time investment and expert knowledge to find relevant data for analysis.
SemantiX is a new project to establish, complement and expand AVHRR time series using Copernicus Sentinel-3 A/B imagery and make them and derived ECVs accessible using a semantic Earth observation (EO) data cube. To the best of our knowledge, SemantiX will establish the first EO data cube based on semantically-enriched AVHRR imagery and has the potential to open the AVHRR archive and derived ECVs to a wider audience. Data cube technologies are a game changer for how EO imagery are stored and accessed, but more importantly in how they establish reproducible analytical environments for queries and information production and in how they can better represent multi-dimensional systems. A semantic EO data cube is a spatio-temporal data cube containing EO data, where for each observation at least one nominal (i.e., categorical) interpretation is available and can be queried in the same instance. (Augustin et al. 2019). Such a tool facilitates easier data access for scientists and, in this case, will join the backend of a smartphone application providing visualisation targeted to non-expert users. Offering analysis ready data (i.e., calibrated and orthorectified AVHRR data) in a data cube along with semantic enrichment reduces barriers to conducting spatial analysis through time based on user-defined AOIs and improves data access by enabling queries of image content instead of being limited to querying imagery based on when images were acquired and the area covered. The proposed data cube of AVHRR and Sentinel-3 imagery, and derived-information including selected ECVs (i.e., snow cover extent, lake surface water temperature, vegetation dynamics) will be linked to a mobile citizen science smartphone application. For the first time, various target groups will have a new, direct and interactive access point and simplified access to EO imagery and derived information, including ECVs. Scientists from disciplines unrelated to remote sensing, students (i.e., the next generation of scientists) as well as interested members of the public will have direct access to long EO data time series for a variety of applications and location-based access through the mobile citizen science application. SemantiX runs from August 2020-2022 funded by the Austrian Research Promotion Agency (FFG) under the Austrian Space Applications Programme (ASAP 16) (project # 878939) in collaboration with the Swiss Space Office (SSO).
This contribution presents a prototypical semantic EO data cube containing a short, temporal subset of AVHRR imagery (updated after Hüsler et al. 2011). The AVHRR time-series has been semantically-enriched using the Satellite Image Automatic Mapper (SIAM). SIAM applies a fully automated, spectral rule-based routine based on a physical-model to assign spectral profiles to colour names with known semantic associations; no user parameters are required, and the result is application-independent (Baraldi et al. 2010). Existing probabilistic cloud masks generated by the Remote Sensing Research Group (Musial et al. 2014) are also included in the semantic EO data cube as additional data-derived information to support spatio-temporal semantic queries. This prototypical implementation is a very first step towards the overall objective of combining climate-relevant AVHRR time series with Sentinel-3 imagery for the Austrian-Swiss alpine region, a European region that is currently experiencing serious changes due to climate change that will continue to create challenges well into the future.

REFERENCES

Augustin, H., Sudmanns, M., Tiede, D., Lang, S., & Baraldi, A. 2019: Semantic Earth Observation Data Cubes. Data, 4(3), 102. https://doi.org/10.3390/data4030102

Baraldi, A., Durieux, L., Simonetti, D., Conchedda, G., Holecz, F., & Blonda, P. 2010: Automatic Spectral-Rule-Based Preliminary Classification of Radiometrically Calibrated SPOT-4/-5/IRS, AVHRR/MSG, AATSR, IKONOS/QuickBird/OrbView/GeoEye, and DMC/SPOT-1/-2 Imagery—Part I: System Design and Implementation. IEEE Transactions on Geoscience and Remote Sensing, 48(3), 1299–1325. https://doi.org/10.1109/TGRS.2009.2032457

Bojinski, S., Verstraete, M., Peterson, T. C., Richter, C., Simmons, A., & Zemp, M. 2014: The Concept of Essential Climate Variables in Support of Climate Research, Applications, and Policy. Bulletin of the American Meteorological Society, 95(9), 1431–1443. https://doi.org/10.1175/BAMS-D-13-00047.1

Hüsler, F., Fontana, F., Neuhaus, C., Riffler, M., Musial, J., & Wunderle, S. 2011: AVHRR Archive and Processing Facility at the University of Bern: A comprehensive 1-km satellite data set for climate change studies. EARSeL EProceedings, 10(2), 83–101.

Musial, J. P., Hüsler, F., Sütterlin, M., Neuhaus, C., & Wunderle, S. 2014: Probabilistic approach to cloud and snow detection on Advanced Very High Resolution Radiometer (AVHRR) imagery. Atmospheric Measurement Techniques, 7(3), 799–822. https://doi.org/10.5194/amt-7-799-2014

20.3
Morphology of rafted blocks in a buried landslide: A case study from the Exmouth Plateau, offshore NW Australia

Ovie Emmanuel Eruteya[1], Yakufu Niyazi[2], Kamaldeen Olakunle Omosanya[3] & Daniel Ierodiaconou[2], Andrea Moscariello[1]

[1] *Department of Earth Sciences, University of Geneva, Rue des Maraîchers 13, CH-1205 Genève (ovie.eruteya@unige.ch)*
[2] *School of Life and Environmental Sciences, Centre for Integrative Ecology, Deakin University, Warrnambool, Victoria, 3280, Australia*
[3] *OASISGEOKONSULT, 7052, Trondheim, Norway*

Submarine mass wasting plays a vital role in remobilizing substantial volumes of sediments basinward including massive slide blocks from the continental shelves and/or upper slope into deeper water. Landslides are notorious for damaging vital subsea infrastructure, triggering tsunamis and problematic during offshore drilling operations for hydrocarbon exploration. Yet, the understanding of the evolution of slide blocks and their associated deformations during downslope transportation remains limited, particularly in data-starved deep-water settings. In this study, we investigated the morphology of large blocks preserved in a buried landslide in the Exmouth Plateau, offshore NW Australia using a 2D and 3D seismic reflection data (Figure 1).

Analysis of the dataset revealed a buried landslide, termed MTC-BDF spanning ~75 km by ~35 km and containing at least 32 blocks (inside the 3D seismic coverage) surrounded by a well-deformed debrite background (Figure 1 and 2a and c). The evolution of this paleo-landslide is related to instability along the slope and flanks of an underlying Miocene submarine canyon (Figure 1). These blocks construed as rafted blocks have lengths ranging from 0.48 km to 3.40 km with thicknesses reaching up to 165 m (Figure 2a, c-g). Interestingly, these blocks are more abundant in a region characterized by moderate-high amplitude debrites (Figure 2c). Erosional morphologies encompassing a unique groove and other circular to irregular-shaped depressions mapped along the basal shear surface provide evidence for the erosive nature of the flow (Figure 2b). The origin of the groove is related to transported blocks gouging the basal shear surface. Importantly, intra block deformations are recorded within these blocks as fault and fold systems (Figure 2d-e). This suggest a complex flow regime within MTC-BDF, with the deformations arising either during block translation or also possibly upon the arrest of the failed mass in interaction with bathymetric elements. Our findings suggest inherent deformations within these blocks may serve as high-permeability conduits with implications for deep-water drilling operations within this segment of the Exmouth Plateau and elsewhere in other hydrocarbon-rich deep-water settings.

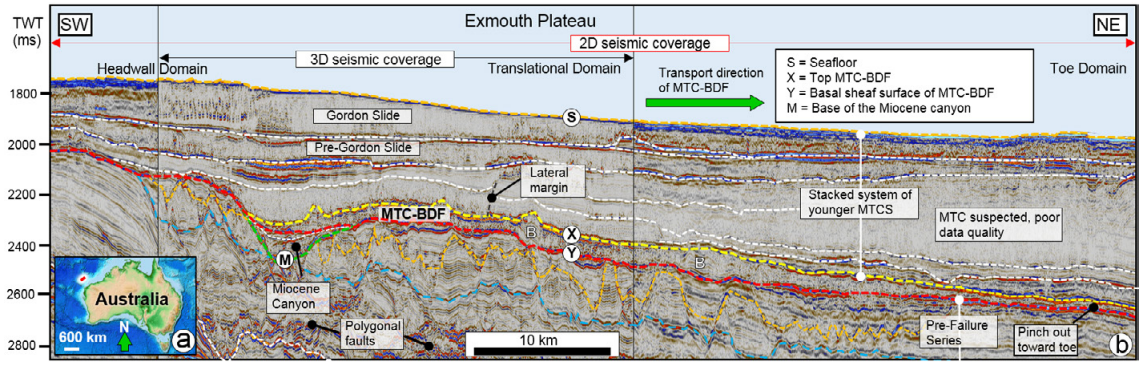

Figure 1. Study area. (a) Location map of the study area in context of offshore NW Australia. Study area is denoted by the red rectangle (b) Structure of the study area in the Exmouth Plateau. The interpreted seismic line shows the Neogene successions of Exmouth Plateau is characterized by the emplacement of stacked system of mass transport complexes from Miocene to recent. The focus of this study is the buried MTC-BDF bounded by Horizon X and Y. B denote slide block.

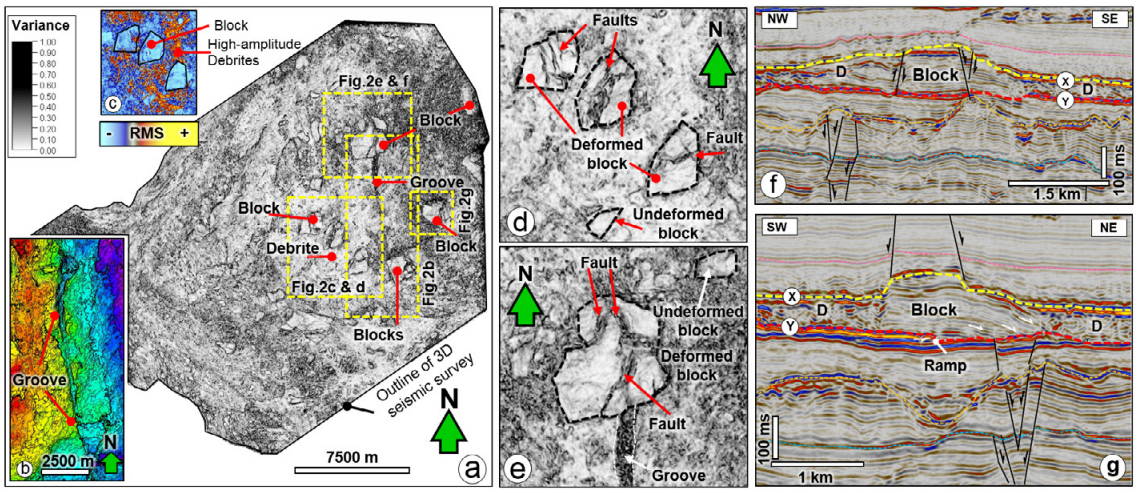

Figure 2. Internal architecture of MTC-BDF (a) Variance attribute slice generated from 3D seismic data flattened along the BSS (Horizon Y) at -2320 ms TWT. The blocks within MTC-BDF are well imaged within the debritic matrix background. (b) A unique erosional groove along the basal shear surface developed by tooling activities of block fragments (see figure 2a for location). (c) RMS attribute of parts of MTC-BDF showing blocks surrounded by high-amplitude debrites. (d-e) Enlarged deformed and undeformed blocks within MTC-BDF as shown in the variance slice (see figure 2a for location). Remnant of the groove is likewise visible (see figure 2b). (f-g) Rafted blocks in MTC-BDF. Seismic sections showing the internal configuration of MTC-BDF comprising of blocks and debrites. Some of these blocks show internal deformation characterized by faults and discordant relationships with the BSS where ramps are present. Location of seismic profiles is shown in figure 2a. In all figures D denote debrites within MTC-BDF.

20.4
Measing surface displacements using a novel UAV/car-borne radar interferometer: including a case study on a fast-moving landslide in Brinzauls

Othmar Frey[1] / [2], Charles L. Werner[1], Andrea Manconi[1], Roberto Coscione[2]

[1] Gamma Remote Sensing, Worbstrasse 225, CH-3073 Gümligen (frey@gamma-rs.ch)
[2] ETH Zurich, Earth Observation & Remote Sensing, Institute of Environmental Engineering, Leopold-Ruzicka-Weg 4, CH-8093 Zurich.

Synthetic aperture radar (SAR) interferometry based mobile mapping of ground surface displacements from moving sensor platforms such as cars and UAVs has been a rather unexplored field. In our contribution we address this topic comprehensively and, particularly, we demonstrate InSAR-based measurement of surface displacements with our newly developed car-borne and UAV-borne L-band SAR system at different test sites in Switzerland.

The reduced temporal decorrelation at L-band is an important advantage and a complementary property as compared to high-frequency (quasi-)stationary systems. While the sensitivity to line-of-sight displacements is lower, the longer wavelength permits to acquire longer interferometric time intervals also in natural terrain and even in adverse conditions (rain, snowfall), in which the decorrelation time at X- or Ku-band (the frequencies of many stationary terrestrial radar interferometers) can be in the order of minutes or less.

Terrestrial SAR data acquisitions from a car driving on a road or imaging from a UAV allow synthetic aperture lengths of 100m and longer, which means that high-resolution SAR imagery can also be obtained at lower frequencies such as L-band. In addition, view geometries (line-of-sight views to landslides) complementary to those available from spaceborne SAR systems can be selected. A flexible SAR imaging approach (time-domain back-projection) allows that even for curvilinear sensor trajectories (e.g. a car driving along a curved road) high-quality SAR images and repeat-pass interferograms with good spatial resolution are obtained.

We show based on a few test sites that such a mobile InSAR system fills a current gap in terms of available InSAR systems for displacement monitoring. A particular focus is laid on a case study carried out on a fast moving landslide in Brinzauls (GR), Switzerland, for which the entire processing approach/chain including mitigation of the tropospheric phase variations is discussed (see also Fig. on next page). We highlight the potential and discuss the challenges and the limitations of this novel InSAR-based mobile mapping system.

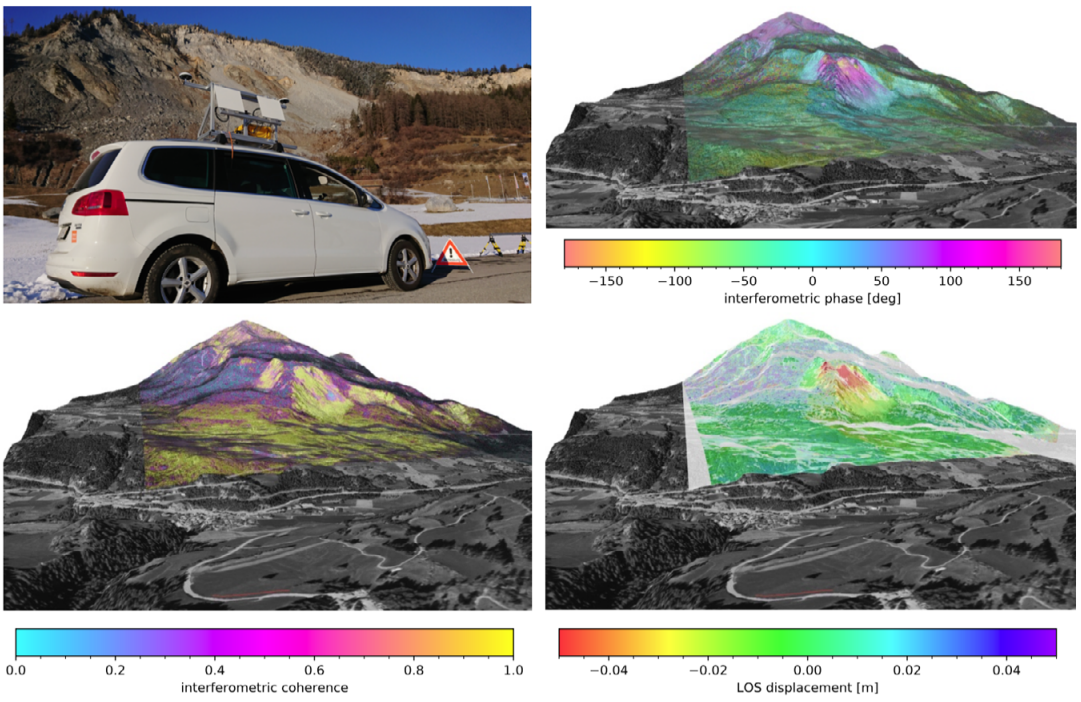

Top left: Car-borne SAR setup with the novel compact L-band FMCW SAR system at test site Brinzauls, Switzerland, where a fast-moving land slide was observed. 4-day repeat-pass interferogram (top right), coherence (lower left), and relative line-of-sight (LOS) displacement (lower right) after unwrapping, atmospheric phase detrending, and coherence & shadow masking (whitish blend). The track of the car-borne SAR acquisitions is indicated with a red line close to the view point.

20.5
Remote sensing of sun-induced fluorescence in inland and coastal waters: current state and future prospects

Remika Gupana[1,2], Daniel Odermatt[1,2] & Alexander Damm-Reiser[1,2]

[1] Department of Surface Waters - Research and Management, Eawag - Swiss Federal Institute of Aquatic Science and Technology, Ueberlandstrasse 133, CH-8600 Duebendorf (remika.gupana@eawag.ch)
[2] Department of Geography, University of Zurich, Winterthurerstrasse 190, CH-8057 Zurich

Sun-induced fluorescence (SIF) emission can be used as a proxy for chlorophyll-a concentration and as indicator of phytoplankton physiological status. The traditionally used fluorescence line height algorithm to measure SIF shows various limitations to adequately account for the low magnitude and dynamic characteristic of this naturally occurring signal. Besides physiological factors, optical properties of the atmosphere and the water body, instrumental effects, and assumptions inherent to retrieval schemes complicate the retrieval and interpretation of SIF. Thus, the complexity of factors determining SIF occurrence and measurement causes SIF to be under-exploited, particularly in inland and coastal waters.

In this study, we address the need to examine the current state of SIF remote sensing in optically complex waters, where the gaps are and how future missions can advance this field of research. We review the theory behind SIF occurrence, available instrumentation to measure water leaving radiance, retrieval schemes to disentangle SIF from other non-SIF contribution to upwelling radiance, and how the subsequent results can be applied in lacustrine and coastal waters.

The Fluorescence Explorer (FLEX) is an upcoming satellite mission dedicated to measure terrestrial SIF globally. FLEX, currently under development by the European Space Agency, will fly in tandem with Sentinel-3 and is planned to be launched in 2023. This tandem mission offers a new generation of data which can advance SIF research in inland and coastal waters. We confront challenges identified in our review with the capacity of this new mission. We particularly evaluate possibilities to better constrain SIF retrievals and how FLEX data can improve interpretation of retrieved SIF. Moving forward, we can conduct further investigation on how to fine-tune SIF estimation knowing the characteristics of the FLEX payload. We can also assess how improved SIF emission estimates can advance applications in biomass estimation, phytoplankton taxonomic discrimination and primary productivity modelling.

20.6
Geostatistical downscaling of offshore coarse spatial resolution wind speed data using satellite-derived wind information

Stylianos Hadjipetrou[1,2], Phaedon Kyriakidis[1], Gregoire Mariethoz[2]

[1] Department of Civil Engineering and Geomatics, Cyprus University of Technology, 2-8 Saripolou, 3036 Limassol, Cyprus (sk.hadjipetrou@edu.cut.ac.cy)
[2] Institute of Earth Surface Dynamics (IDYST), University of Lausanne, UNIL-Mouline, Geopolis, 1015 Lausanne, Switzerland

Researchers from multiple disciplines rely on routine forecasts from Numerical Weather Prediction (NWP) models to conduct wind resource assessments for wind energy projects. These forecasts are often corrected on the basis of observations via data assimilation methods. The model output products, however, are usually provided at a coarse spatial resolution which in several cases affects the estimation and interpretation process regarding regional or local-scale natural phenomena. Indeed, detailed resource or impact assessment studies often call for higher spatial resolution data products. Remote sensing data e.g. Synthetic Aperture Radar (SAR) on the other hand are typically exploited to retrieve the spatial distribution of wind fields over the sea surface at a high spatial resolution. Sentinel-1A & 1B C-band SAR instruments, in particular, provide detailed information on the spatial variability of offshore wind. Despite the satellite's low repeat frequency, Sentinel-1 data are a valuable source of information for conducting offshore wind resource assessment as well as for the long-term validation of wind speed measurements from various sources.

Downscaling techniques can be performed on spatial and temporal aspects of climate projections in order to obtain higher resolution wind images that could be used for more detailed trend recognition and projection of future phenomena. The methodology of this work is based on a novel geostatistical approach for downscaling the Uncertainties in Ensembles of Regional Reanalyses (UERRA) data using Sentinel-1A & 1B SAR data in order to spatially enhance the coarse information of the former. More precisely, Ocean Wind Fields (OWI) geophysical component data from Sentinel-1 Level-2 Ocean (OCN) products are used primarily with a spatial resolution of 1km to refine the coarse wind information (11km) derived from the UERRA-HARMONIE 3-dimensional variational data assimilation system thus contributing in a more detailed offshore wind speed assessment for Cyprus. Sentinel-1 data have been validated against in-situ data from Cyprus' coastal meteorological stations.

The proposed methodology is showcased via the estimation of offshore wind speed values at a spatial resolution of 1km for the offshore area of Cyprus and at specific dates around the year. Results indicate that the geostatistically downscaled predictions can provide the basis for finely resolved offshore wind resource assessments. The methodology can also be further developed to predict the spatial distribution of wind speed values at a fine spatial resolution for time periods where Sentinel-1 data are not available. Lastly, unlike traditionally employed methods where the uncertainty is based on a per-pixel analysis, our method quantifies the uncertainty of the gridded estimates collectively.

20.7
How small can ground movements be in order to be detected with GNSS?

Hohensinn R., Rothacher M.

Institute of Geodesy and Photogrammetry, ETH Zurich, Robert-Gnehm-Weg 15, CH-8093 Zurich

High-precision GNSS (Global Navigation Satellite System) positioning can reach an accuracy down to the millimeter level, and typically ground motions down to tenths of millimeters per year can be resolved. This paper addresses the sensitivity of GNSS for the resolution of medium and long-term movements, as observed for plate motions, postglacial uplift, or the motions of rock glaciers, for example. For our analysis, the data comes from the GNSS stations of the EPN (European Permanent Network) – the GNSS station coordinates are obtained at a daily sampling rate, with almost 25 years of data available for some stations. Based on these time series data, we use a common mathematical model, that accounts for long-term station drift, annual- and semiannual variations, as well as for discontinuities (sudden jumps). Together with a statistical description of the GNSS observation noise we set up an a-priori adjustment model, based on which we are deriving the parameters of target, namely minimum detectable displacements for the long-term drift, the periodic seasonal variations and the discontinuities.

We see that the minimum detectable displacements depend strongly on the length of the time series and on the noise characteristics. Furthermore, an important quantity is the number of discontinuities that result, e.g., from GNSS equipment changes or earthquakes. For GNSS stations with good performance, the displacements that can be detected are at the level of few millimeters or even below.

We conclude that such an analysis can be useful for global change monitoring with GNSS, and it can be used to determine how long one has to observe in order to detect critical phenomena. Furthermore, the methodology can be applied not only in the field of GNSS but also to any other remote sensing technique.

20.8
Efficient high-density bird colony censuses using drones and convolutional neural networks

Benjamin Kellenberger[1,2], Thor Veen[3], Eelke Folmer[4], Devis Tuia[2]

[1] Wageningen University, Wageningen, the Netherlands (benjamin.kellenberger@wur.nl)
[4] Environmental Computational Science and Earth Observation Laboratory, Ecole Polytechnique Fédérale de Lausanne (EPFL), Switzerland (devis.tuia@epfl.ch)
[3] Quest University, 3200 University Blvd, Squamish, BC V8B 0N8, Canada
[4] SkyPilot UAS

The West-African coastline offers suitable breeding conditions for colonial breeding bird species like the African Royal Tern (*Thalasseus maximus albididorsalis*), Caspian Tern (*Hydroprogne caspia*), Slender-billed gull (*Chroicocephalus genei*), and Gray-headed gull (*Chroicocephalus cirrocephalus*). To evade predation and disturbance they breed on sandy islands where they form large breeding colonies. However, the number of undisturbed breeding islands is limited and the four species thus highly sensitive to changes such coastal erosion and disturbance (Veen et al., 2019). Mapping and counting bird colonies is a vital necessity for conservation purposes. However, manual counting is a complex task, due to high population densities in the limitedly sized breeding spots.

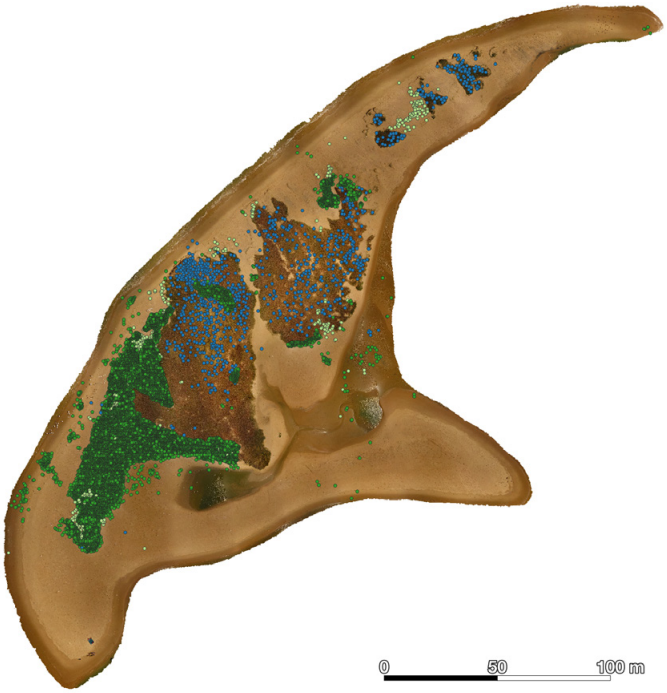

Figure 1: High-resolution test orthomosaic with 21›066 manually annotated bird individuals.

In this work, we aim at automatically identifying, classifying, and counting colonies of birds using drone imagery and Convolutional Neural Networks (CNNs; Zhu et al., 2017). In a first instance, we acquired six high-resolution (1cm) orthomosaics along the West African coast in May 2019, using a DJI Phantom 4 drone[1]. These were then labeled with point annotations and species information in a locally complete manner, *i.e.*, all individuals were annotated in small regions, but not necessarily across the entire images. We deliberately allowed incomplete annotations that did not include all individuals present in an image to facilitate the manual labeling task as much as possible. One orthomosaic was fully annotated and served for accuracy evaluation only (Figure 1). The open source software AIDE was used to create the annotations[2].
We then trained a CNN based on a ResNet-18 (He et al., 2015) that predicts a patch-wise grid of bird species probabilities as described in Kellenberger et al. (2018). A Markov Random Field was further employed to improve prediction quality in terms of spatial patterns (Li, 2012).

[1] https://www.dji.com/ch/phantom-4
[2] https://github.com/microsoft/aerial_wildlife_detection

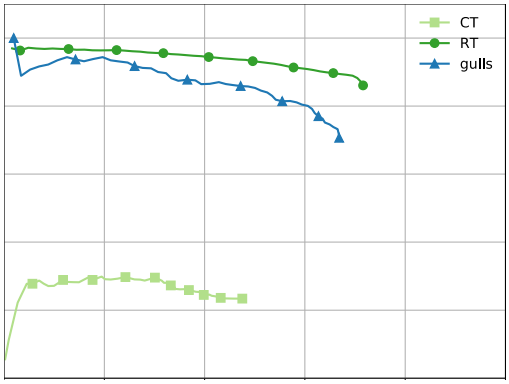

Figure 2: Our CNN detects birds with high precision and recall, but only requires 200 training points per species and three hours for training.

Our test orthomosaic contains 21’066 point annotations, which were created by five experts in three working hours spread across several weeks. In contrast, our CNN only required 200 point annotations per species and a low number of drawn background polygons for training and predicted 23’288 birds with a high precision and recall (Figure 2). In sum, our model reduces the required analysis time for bird censuses by orders of magnitude, and relieves operators from the tedious manual labeling of high-density bird colonies.

REFERENCES

He, K., et al. 2015: Deep residual learning for image recognition. IEEE CVPR.

Kellenberger, B., Marcos, D., & Tuia, D. 2018: Detecting mammals in UAV images: Best practices to address a substantially imbalanced dataset with deep learning. Remote sensing of environment 216, 139-153.

Li, SZ 2012: Markov random field modeling in computer vision. Springer Science & Business Media.

Veen, J., et al. 2019: Diet and foraging range of slender-billed gulls Chroicocephalus genei breeding in the Saloum Delta, Senegal. Ardea 107.1, 33-46.

Zhu, XX, et al. 2017: Deep learning in remote sensing: A comprehensive review and list of resources. IEEE Geoscience and Remote Sensing Magazine 5.4, 8-36.

20.9
Monitoring displacements of complex landslide scenarios with broadband multiplatform radar techniques

Andrea Manconi*, Rafael Caduff*, Tazio Strozzi*, Othmar Frey*, Charles Werner*, Urs Wegmuller*

[1] GAMMA Remote Sensing, Worbstrasse 225, Geumligen, Switzerland, www.gamma-rs.ch *(*manconi@gamma-rs.ch*)*

The evolution of slope instabilities towards catastrophic failure events is accompanied by the progressive increase of ground displacements. For this reason, accurate data of surface deformation in space and time is important for the analysis and the interpretation of the associated hazard and risk potential. Remote sensing techniques have demonstrated to be a valid complement to standard in-situ monitoring. In particular, Differential Synthetic Aperture Radar Interferometry (DInSAR) from satellite-based imagery as well as from ground-based platforms allowed great advances in the identification and monitoring of surface deformation processes. However, the results obtained with currently available DInSAR methods might be hindered by insufficient spatial or temporal resolutions and/or due to intrinsic limitations of the methods used. For example, satellite based DInSAR provides great advantages to cover large areas, identify and map landslide displacements, and to monitor their spatial and temporal evolution in periods ranging from days to years. Despite, when the scenario evolves towards a potential failure, revisit times in the order of several days are not sufficient anymore. Phase aliasing, decorrelation, geometrical distortions, and layover/shadowing effects typical of satellite acquisitions may additionally hamper the possibility of accurate interpretations. On the other end, terrestrial based radar systems provide higher sensitivity to very small movements and are generally used when the landslide scenario requires continuous monitoring. These devices can obtain representative information over the area of interest, however, their spatial coverage is often limited and, since they exploit Ku- or X-band wavelengths, may suffer when large surface displacements occur. For this reason, comprehensive analyses of surface displacements should imply the use of multiple interferometric radar datasets. Here we present the results of an integrated investigation performed in Brienz/Brinzauls, GR, Switzerland. There, an area of 3 km2 is affected by a large and complex compound landslide with surface velocities locally exceeding values of 1 m/year. The scenario poses high concerns to the community, first for the village directly affected by extensive damage to the buildings (some of them already evacuated for safety), and more in general for the transportation network lines that would be affected in case of catastrophic failure. We selected analyzed SAR data acquired from: (i) satellite platforms, Sentinel-1 (C-Band) and ALOS-2 (L-Band); (ii) ground-based GAMMA Portable Radar Interferometer (GPRI, Ku-Band) from different locations; (iii) Car-borne SAR L-Band imagery, acquired from similar locations as the GPRI. We explore the results of interferometric analyses considering different observation periods and weather conditions.

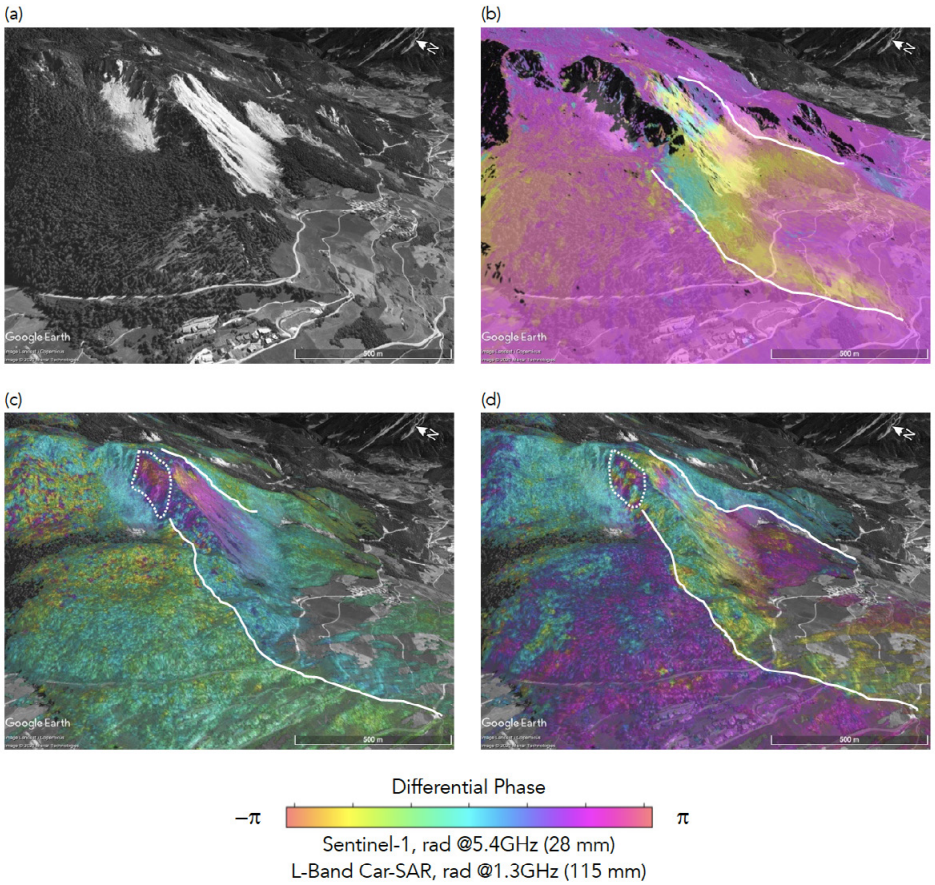

Figure 1. Comparison between the results obtained from car-borne and Satellite radar interferometry. (a) Background reference (Google Earth); (b) Sentinel-1 interferogram between January 08 and January 14, 2020, ascending orbit; (c) Car-borne interferogram between 20 and 24 January, 2020, both acquisitions in clear weather conditions; (d) Car-borne interferogram between 20 January and 3 February, 2020, with the second acquisition performed in rainfall conditions. Note that the area bounded with white dashed lines in (c) and (d) is not visible in (b) because of layover/shadowing effects due to the Sentinel-1 acquisition geometry.

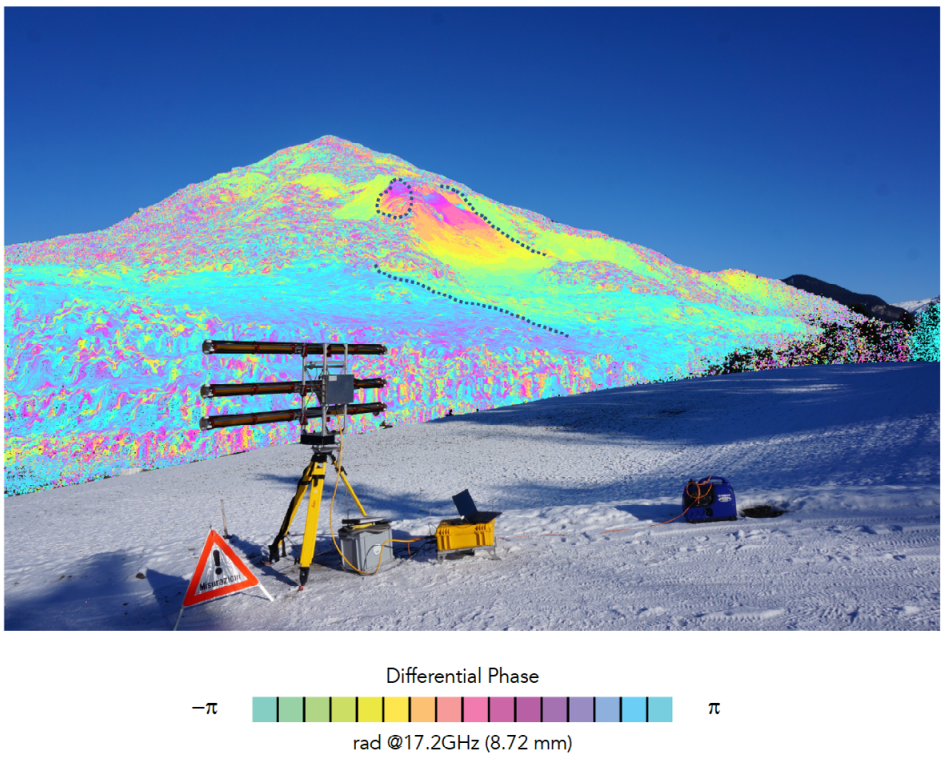

Figure 2. Results obtained with the GPRI system on January 22, 2020 between 10:46 and 18:19 overlain on a picture of the Brienz/Brinzauls slope. Black dashed lines mark the zones of phase gradients associated with areas having different displacement behavior. These areas match well with the results obtained with the space-borne and the car-borne interferometric results.

20.10
Atmospheric tomography – a valuable asset for future CubeSat missions

Gregor Moeller[1], Chi O. Ao[2]

[1] ETH Zürich, Institute of Geodesy and Photogrammetry, Robert-Gnehm Weg 15, 8093, Zürich, Switzerland (gmoeller@ethz.ch)
[2] NASA Jet Propulsion Laboratory, California Institute of Technology, 4800 Oak Grove Drive, 91011, Pasadena, California, USA

Recent developments in small-satellite technology open up new possibilities for Earth observation. We expect that in the next decade large CubeSat constellations will arise with hundred, up to thousand satellites in low Earth orbit. While most constellations will be dedicated to internet of things and global communication, a larger number of satellites might be also equipped with rather low-cost sensors – suited for monitoring of the Earth's atmosphere. In this context, the GNSS radio occultation (RO) technique has been identified as a promising tool for remote sensing of the atmospheric state. For processing of the RO signals, a new analysis method has been developed, which is based on tomographic principles.

In this presentation, we will highlight the basic principles of the developed approach and will show a series of closed-loop validations to demonstrate the potential of tomographic techniques for analysis of dense CubeSat constellations. Applied to GNSS signal delays it will allow for a detailed reconstruction of the water vapour distribution inside and outside convective systems and therefore, will contribute to a better understanding of convective storms, heavy precipitation and related weather events.

20.11
Refinement of CubeSat orbit determination using on-board velocity solutions

Lukas Müller[1], Kangkang Chen[1] & Markus Rothacher[1]

[1] *Institute of Geodesy and Photogrammetry, ETH Zurich, Robert-Gnehm-Weg 15, CH-8093 Zurich (lukamueller@ethz.ch)*

In December 2018 and April 2019, two 3-unit cube satellites of the company Astrocast were launched into space. Both satellites are equipped with our low-cost single-frequency multi-GNSS payload board, which can provide continuous on-board navigation solutions containing position, velocity and time. By fitting a dynamic orbit to these on-board solutions using the Bernese GNSS Software, we can evaluate the quality of the on-board solutions. Usually, only the receiver positions of the satellite are used to fit a dynamic orbit without considering the receiver velocity information that is also available. In this study, we develop and analyse an extension and refinement of the dynamic orbit determination by using not only the satellite positions but also the satellite velocities of the on-board solution in the orbit fit.

To study the use of velocity observations in the determination of a precise dynamic orbit, we consider three different approaches: fitting the equation of motion of the satellite orbit (1) to the positions only, (2) to the velocities only and (3) to both positions and velocities. For the combined orbit estimation with positions and velocities, we apply an appropriate relative weighting of the two observation types based on the RMS of the residuals from the orbit fits.

After removing a few outliers, the standard deviation of the position residuals from the position-only approach is about 5 m, the standard deviation of the velocity residuals from the velocity-only approach is about 15 cm/s. However, when looking at the positions computed from the velocity-only approach they deviate by much more than a few meters from the orbit obtained by the position-only fitting. These deviations show a periodicity of one revolution with an amplitude of up to 60 m. In the differences between the velocity-only and position-only orbit fit we see an offset of about -0.01 m/s in the radial component of the velocities and an offset of about 15 m in the along-track component of the positions. Additionally, a periodicity of one revolution with an amplitude of 0.03 m/s to 0.05 m/s is detected in the differences of all velocity components.

These discrepancies between the different approaches indicate that considerable systematic effects must be present in the receiver solutions. Apart from the ionospheric refraction that leads to a radial position bias in the satellite orbit, we also expect systematic effects from the receiver tracking loops under the high dynamics and from the deficiencies in the modelling of the perturbing forces acting on the satellite. With a detailed analysis of the three approaches over a long time span, we quantify these inconsistencies and identify their causes.

20.12
SenCast: Instant Copernicus satellite data and analysis

Daniel Odermatt[1,2], James Runnalls[1], Joan Tracy Sturm[2] & Alexander Damm[1,2]

[1] Eawag, Swiss Federal Institute of Aquatic Science and Technology, Ueberlandstrasse 133, CH-8600 Duebendorf (daniel.odermatt@eawag.ch)
[2] Department of Geography, University of Zurich, Winterthurerstrasse 190, CH-8057 Zurich

This contribution was recently published in Geomatik Schweiz as: 'SenCast: Copernicus Satellitendaten auf Knopfdruck' [in German].

The Sentinel satellites by the European Copernicus program have provided standardized data for environmental monitoring since 2014. For example, Sentinel-3 and Sentinel-2 acquire spatially and spectro-radiometrically detailed imagery with global coverage within one and five days, respectively. Access to this data is open and free of charge via conventional archives of the European Space Agency (ESA) and EUMETSAT, via five Data and Information Access Services (DIAS) commissioned by the European Union, or via third-party providers. The availability of these extensive datasets requires however dedicated tools and analysis strategies for automated and harmonized processing. Availability of such tailored tools is, still limited and their use is often complicated.

With the financial support of the Federal Office for the Environment, we developed the open source software package SenCast. SenCast is a versatile tool that can be used in all fields of environmental Earth observation (Odermatt et al., 2020; https://gitlab.com/eawag-rs/sencast). It is implemented in Python, and independent of operating systems. SenCast is entirely based on open source software and on processors from the Sentinel Application Platform (SNAP, https://step.esa.int), an open source toolbox from ESA. SenCast is developed to automatically process historical data, or new data as soon as they become available in archives (e.g. ESA, EUMETSAT, various DIAS).

In this study, we outline the functioning and structure of SenCast and we demonstrate its applicability for environmental research on aquatic and terrestrial ecosystems. Exemplarily, we show how SenCast enables assessments of primary production and summer calcite precipitation (Nouchi et al., 2019) using chlorophyll-a, Secchi depth and turbidity estimates from Sentinel-3 data. Another example relates to a recently reported forest damage due to extreme weather conditions in the summer of 2018 (Schuldt et al., 2020). We use SenCast to calculate proxies sensitive to dynamics in plant water content from Sentinel-2 data, and use these proxies to evaluate the severity and extent of damages across Switzerland. SenCast can be installed on desktop computers, DIAS platforms or other servers. It is configured using simple text-based parameter definitions, and it can be extended by users who have basic knowledge of Python and SNAP or XML. We also show how products generated with SenCast will be made accessible in a new information portal on the state of Swiss waters (https://www.datalakes-eawag.ch).

REFERENCES

Nouchi, V., Kutser, T., Wüest, A., Müller, B., Odermatt, D., Baracchini, T., and Bouffard, D. (2019). Resolving biogeochemical processes in lakes using remote sensing. Aquatic Sciences 81(2), 27.

Odermatt, D., Runnalls, J., Sturm, J.T., and Damm, A. (2020). SenCast: Copernicus Satellitendaten auf Knopfdruck [in German]. Geomatik Schweiz 5.

Schuldt, B., Buras, A., Arend, M., Vitasse, Y., Beierkuhnlein, C., Damm, A., Gharun, M., Grams, T.E.E., Hauck, M., Hajek, P., et al. (2020). A first assessment of the impact of the extreme 2018 summer drought on Central European forests. Basic and Applied Ecology.

20.13
Typical Uncertainties in Measurements of Leaf Optical Properties Still Permit Detection of Fine-Scale Biological Variation

Fanny Petibon[1], Ewa Czyz[1], Giulia Ghielmetti[1], Andreas Hueni[1], Mathias Kneubühler[1], Michael E. Schaepman[1], Meredith C. Schuman[1,2]

[1] Department of Geography, University of Zürich, Winterthurerstrasse 190, CH-8051 Zürich (fanny.petibon@geo.uzh.ch)
[2] Department of Chemistry, University of Zürich, Winterthurerstrasse 190, CH-8051 Zürich

The measurement of leaf optical properties (LOP) supports continuous, time-resolved, and rapid characterization of an increasing amount of ecophysiological information from plant communities. Field spectrometers are widely used to calibrate measurements from airborne optical sensors (Hueni, 2017) or to directly monitor biological variation at the leaf level (Jacquemoud and Ustin, 2019). Coupled with a contact probe and a standardized light source, they allow LOP measurements to be taken independently of environmental conditions and with an expected high accuracy and repeatability. However, to our knowledge, neither standardized nor systematic characterizations exist for the measurement uncertainties associated with commonly used contact probes, i.e., leaf clips and integrating spheres.

In this study we investigate what level of uncertainty can be tolerated in LOP measurements while ensuring reliable information about biological phenomena of interest. We first identify and quantify the uncertainty of measurements from standard materials with different optical properties. We show that although our integrating sphere yields more repeatable measurements on materials with a high specular reflectance component, measurements tend to be more repeatable using our leaf clip on materials with a low specular component. In a series of experiments on the common European beech Fagus sylvatica, we quantify the amount of variation in LOP associated with biologically distinct groups, i.e., leaves sampled at different times of the season from one individual, or standardized leaves measured within a short time frame from different individuals in a set of monitored Swiss forest stands and in a French forest reserve. Spectral variance in LOP among sun-exposed and fully developed leaves of a single individual, approximated by the coefficient of variation, reaches up to 32% in the visible region, representing more than 90% of the observed coefficient of variation between individuals at corresponding wavelengths (Figure 1). Therefore, taking into account biological variation at smaller scales (i.e., individual) appears essential to be able to draw conclusions and confidence intervals at larger scales (i.e., population). We suggest measures towards a standardized protocol to allow rigorous quantification of biological differences via LOP.

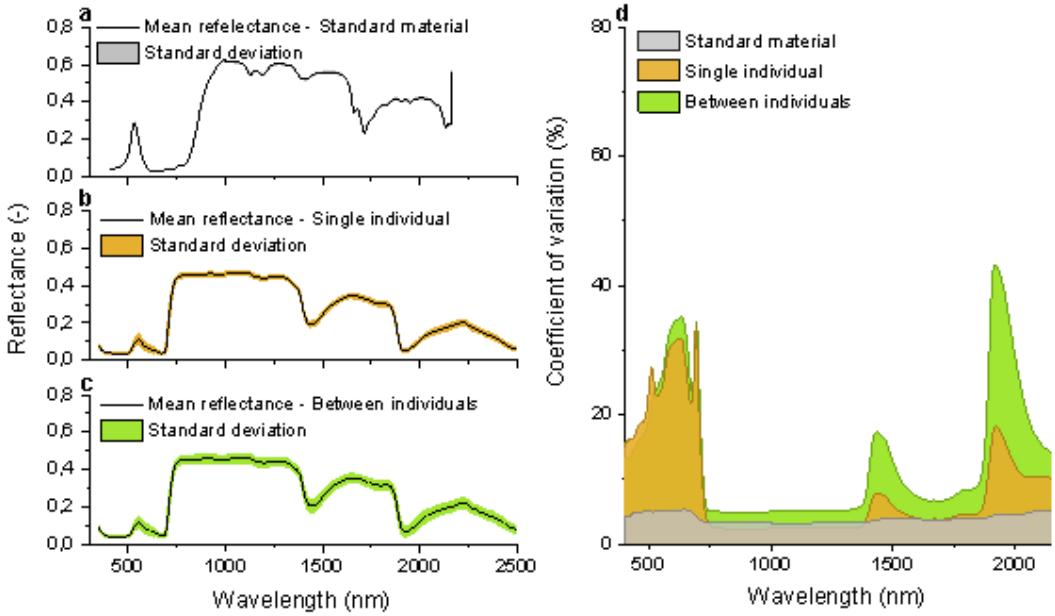

Figure 1. Mean reflectance and standard deviation of a standard material (a), sun-exposed and fully developed leaves of a single individual (b), as well as several individuals (c). The measurement uncertainty is estimated from the coefficient of variation of the standard material and compared to the coefficients of variation of different biological groups to estimate the biological variation (d).

REFERENCES

Hueni, A., Damm, A., Kneubuehler, M., Schläpfer, D., & Schaepman M.E. 2017: Field and Airborne Spectroscopy Cross Validation – Some considerations, IEEE Journal of Selected Topics in Applied Earth Observations and Remote Sensing, 10, 1117-1135.

Jacquemoud, S., & Ustin, S. 2019: Applications of Leaf Optics. In Leaf optical properties, Cambridge: Cambridge University Press, 357-403.

20.14
Comparison of three high resolution real-time spectrometers for microwave ozone profiling instruments

Eric Sauvageat[1,2], Jonas Hagen[1], Mikko Kotiranta[1], Klemens Hocke[1,2], Mike Gomez[3], Gerald Neduloha[3], Axel Murk[1,2]

[1] Institute of Applied Physics, University of Bern, Sidlerstrasse 5, CH-3012 Bern (eric.sauvageat@iap.unibe.ch)
[2] Oeschger Centre for Climate Change Research, University of Bern, Hochschulstrasse 4, CH-3012 Bern
[3] Remote Sensing Division, U.S. Naval Research Laboratory, Washington D.C., USA

Passive microwave ground based radiometry is a remote sensing tool used for the sounding of atmospheric temperatures and the profiling of trace gases such as ozone, water vapor or carbon monoxide. In the case of ozone, this technology provides continuous, all-weather observation capabilities in the middle atmosphere (~25-70km) and is important for estimating long-term trends and cross-validating satellites measurement in this scarce data altitude region.

Today, most atmospheric remote sensing radiometers are using high resolution real-time spectrometers as back-end. While the spectroscopic performance of such back-ends influences the retrieval of atmospheric profiles, their exact contributions are often unknown.

To investigate the performance of different spectrometers for ozone observations, we connect three state-of-the-art spectrometers to the same radiometer front-end for simultaneous operation. We use a single sideband heterodyne receiver with an uncooled low noise amplifier as radiometer front-end (Kotiranta et al., 2019) and the Acquiris AC240, Acquiris U5303 and Ettus USRP X310 as spectrometers (Murk & Kotiranta, 2019). With that instrument, we observe successively a hot and a cold calibration target as well as the atmospheric ozone emission line at 110.8 GHz.

Between January and June 2019, the Microwave Ozone Profiling Instrument (MOPI 5) operated continuously on the roof of the University of Bern (47 °N) in Switzerland and provided parallel observations from the three spectrometers covering a broad band of atmospheric conditions. This setup allows to characterize and compare the radiometric noise performance, channel response, binning artifacts and linearity of the different spectrometers over an extended period of time. We find that the calibrated spectra of the ozone emission line from the AC240 show a systematic bias leading to scaling errors of the observed emission lines. In particular, the spectrum has a systematically smaller line amplitude while its slope, caused by the strong line wing of the oxygen line at 118 GHz, has a different inclination compared to the spectra from the more recent spectrometers U5303 and USRP X310 (Figure 1.). To understand the origin of the observed behavior and characterize this systematic bias, we investigate the influence of these discrepancies to the ozone profile retrieval while taking into account different atmospheric conditions.

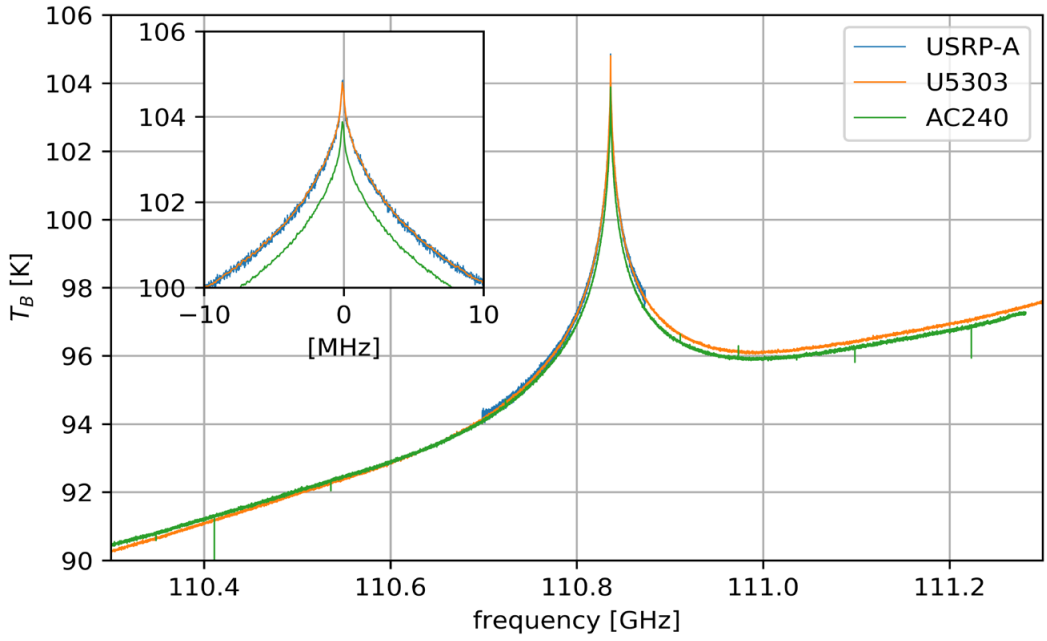

Figure 1. Comparison of a daily calibrated spectra recorded simultaneously on the 4th of January 2019 from the three different spectrometers of the MOPI 5 instrument.

REFERENCES

Kotiranta, M., Gomez, R. M., Nedoluha, G., Kämpfer, N., & Murk, A. 2019: Receiver Development for the Microwave Ozone Profiling Instrument MOPI 5. In IGARSS 2019-2019 IEEE International Geoscience and Remote Sensing Symposium (pp. 8952-8955). IEEE.

Murk, A. & Kotiranta, M. 2019: Characterization of Digital Real-Time Spectrometers for Radio Astronomy and Atmospheric Remote Sensing. In Proceedings of the International Symposium on Space THz Technology, Gothenburg, Sweden (Vol. 15).

20.15
Mapping 3D tropospheric variables in an Alpine Region by collocation of tropospheric delays in spaceborne microwave Signals

Endrit Shehaj[1], Gregor Moeller[1], Alain Geiger[1], Othmar Frey[2,3], Markus Rothacher[1]

[1] *Institute of Geodesy and Photogrammetry, ETH Zürich, Robert-Gnehm-Weg 15, 8093 Zürich, Switzerland (eshehaj@ethz.ch)*
[2] *Institute of Environmental Engineering, ETH Zürich, Zürich, Switzerland*
[3] *Gamma Remote Sensing, Gümligen, Switzerland*

Microwave signals experience delays when traveling through the Earth's atmosphere as a function of the integrated refractivity along the path from the transmitter to the receiver. High spatio-temporal variations in the refractivity index in the troposphere are mainly caused by rapid 4D changes of atmospheric water vapor. These delays affect the output of space geodetic techniques such as Global Navigation Satellite Systems (GNSS) and spaceborne radar interferometry. Consequently, these delays need to be estimated during the processing of the observations, together with the other parametres of interest. Considered a noise in geodetic applications, these estimated delays contain additional information about the tropospheric state, thus tropospheric variables like GNSS Zenith Total Delays (ZTDs) are nowadays routinely assimilated in weather models together with other meteorological parameters. While tropospheric delays are integrated quantities, advanced mathematical methods, such as tomography, are applied to model 3D refractivity fields from tropospheric delays, which can be converted into 3D water vapor or temperature fields.

In this work, we use a collocation framework to model 3D tropospheric quantities. Collocation is an enhancement of traditional parameter estimation and adjustment theory; therefore, we separate the problem into a deterministic and stochastic part and estimate 3D refractivity fields. The used deterministic and stochastic models have been proven accurate in several test campaigns performed by the Institute of Geodesy and Photogrammetry of ETH Zürich.

For validation of the model performance, we focus on an alpine region in Valais, Switzerland, where a relatively dense GNSS network exists, as well as an interferometric time series of Synthetic Aperture Radar (SAR) images is available for several years. After showing the use-case and the available observations, we perform a comparison of our retrieved refractivity fields with a typical tomography approach with the aim to provide a quantitative and qualitative comparison. Furthermore, we investigate the impact of network densification and we display the collocated fields for another region (Upper Rhine Graben) with a very different topography. Finally, we convert our refractivity fields into water vapor and temperature 3D fields, which are Essential Climate Variables (ECVs) directly characterizing the Earth's climate.

20.16
Drought-induced Impacts on Forest Health in Switzerland: A Remote Sensing Perspective

Joan Sturm[1], & Alexander Damm[1]

[1] *Geographisches Institut, University of Zurich, Winterthurerstrasse 190, CH-8057 Zürich (joantracy.sturm@geo.uzh.ch)*

The ongoing warming of Earth's climate has been accompanied by an intensified frequency of extreme events, e.g. droughts, that heavily affect land-atmospheric feedback mechanisms and cycles (Miralles et al. 2019). In Switzerland, the summer of 2018 was the driest summer since 1962 and among the five warmest summers since measurements started (MeteoSchweiz 2019). This combination of low precipitation and high temperatures caused early leaf and needle discoloration, premature leaf-shedding, canopy die-back and tree mortality among many forests (Schuldt et al. 2020).
This study aims to assess the impact and causality of this exceptional event on health and damages in forests across Switzerland. We particularly applied the normalised difference water index (NDWI) (Gao 1996), a topography robust index sensitive for the liquid water content of vegetation canopies and respective changes. The NDWI was parameterized with the Sentinel-2 bands 8 (near infrared) and 11 (shortwave infrared) observed on August 2017, 2018, and 2019. We calculated the normalised difference between the NDWI images over the years to detect the locations and intensities of drought-induced forest changes.
Considering the biogeographic regions of Switzerland, the Jura featured the biggest proportion of negatively affected forest areas, whereas the Central Plateau was least affected (Figure 1). Drought-induced impacts mostly appeared as small isolated patches that as represented by a serious NDWI decrease.

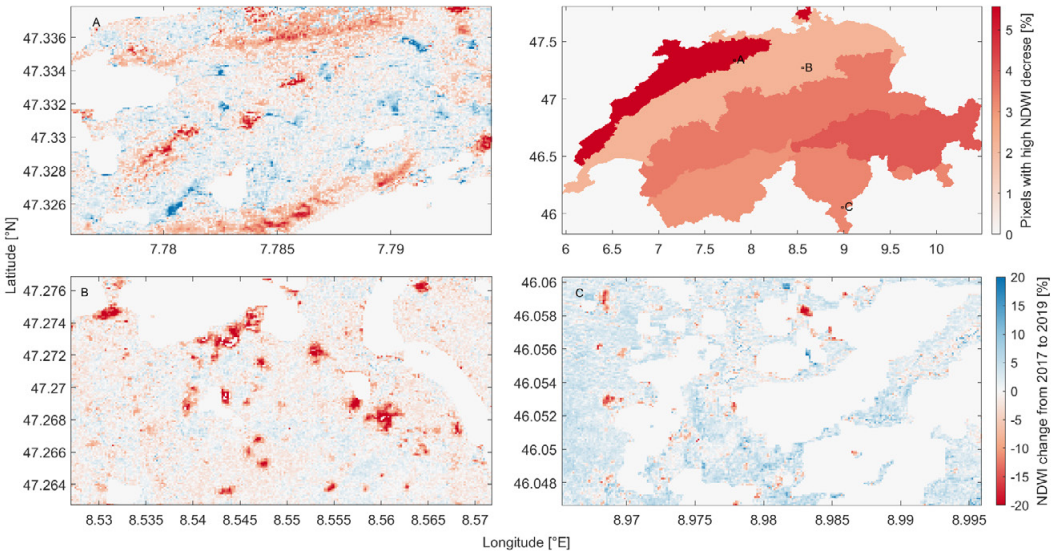

Figure 1. Choropleth map of the biogeographic regions of Switzerland coloured according to their proportion of heavily affected forest areas. Three sites reveal different patterns of change of NDWI values from 2017 to 2019.

A pixel-based analysis was conducted to gain further insight into the causality of forest damage by investigating various environmental parameters. We found a large effect of topographic variables representing the exposition and location of forest. Parts of forests located along ridges suffered more from drought-related damages than forest parts in sheltered locations. Additionally, the mixture and dominant tree species played a crucial role with coniferous trees being more affected than broadleaf trees.

REFERENCES

Gao, B. C. 1996: NDWI - A Normalized Difference Water Index for Remote Sensing of Vegetation Liquid Water from Space, Remote Sensing of Environment, 58(3), 257–66.

MeteoSchweiz 2019: Klimabulletin Sommer 2019, Zürich.

Miralles, D. G., Gentine, P., Seneviratne, S. I., and Teuling, A. J. 2019: Land-Atmospheric Feedbacks during Droughts and Heatwaves: State of the Science and Current Challenges, Annals of the New York Academy of Sciences 1436(1), 19–35.

Schuldt, B. et al. 2020: A First Assessment of the Impact of the Extreme 2018 Summer Drought on Central European Forests, Basic and Applied Ecology 45, 86–103.

P 20.1
Mapping Event Landslides from Satellite Images Using Convolutional Neural Networks

Nikhil Prakash[1], Andrea Manconi[1], Simon Loew[1]

[1] *Engineering Geology, Department of Earth Sciences, ETH Zurich, 8092 Zurich, Switzerland (nikhil.prakash@erdw.ethz.ch)*

An earthquake or an extreme meteorological occurrence in mountainous regions can trigger hundreds of landslides. These event landslides can cause widespread destruction to infrastructure and human lives. Hence, an inventory of landslides triggered by such an event is required to plan a quick disaster response. These event landslides are mapped by identifying characteristic changes in surface features that are associated with ground movements. A pair of satellite images acquired before and after the trigger event is an ideal data source for mapping over large areas. Fully automated machine learning strategies have been studied in this context, as using manual effort is a slow and time-consuming process.

In this work, we develop a new convolutional neural network (CNN) method to map landslides from a pair of satellite images. A modified U-Net architecture was used for the semantic segmentation of EO data. We achieved F1 scores from 0.58 to 0.82 for experiments conducted on multiple earthquakes and metrological triggering events. Figure 1 shows one such mapping result from the 2018 Hokkaido earthquake in Japan. We also explore the option of combining the landslide inventories from multiple events for training. The CNN trained with combined inventories was observed to have better generalization ability, and this eliminates the need of training of a new model after every future events.

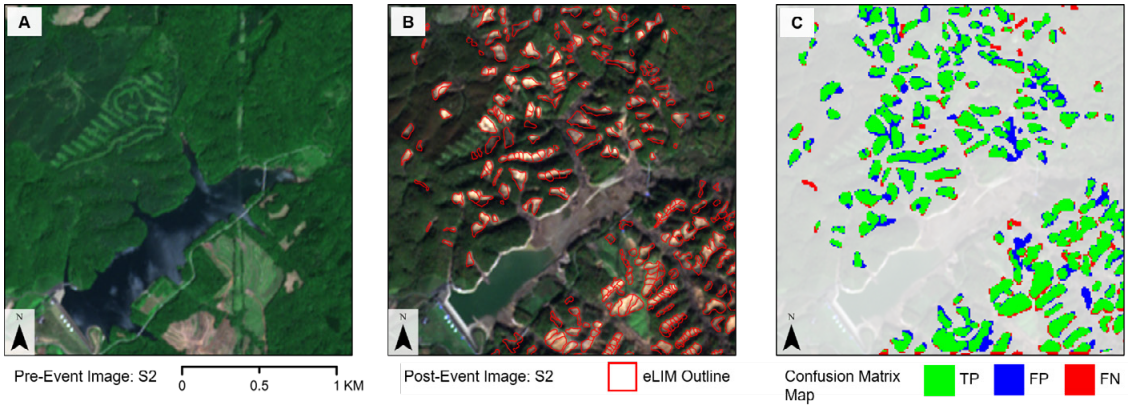

Figure 1. Mapping of landslides triggred by a earthquake in Hokkaido, Japan using the trained CNN. The images from left to right are: (A) pre-event Sentinel-2 image, (B) post-event Sentinel-2 image with landslides inventory from Wang et al. (2019) shown as red polygons, and (C) map of confusion matrix values generated from the output of the CNN. The output from the CNN is compared with the ground truth inventory to generate the confusion matrix map, which shows the true positive (TP), false positive (FP), and false negatives (FN) detections.

REFERENCES

Wang, F., Fan, X., Yunus, A.P., Subramanian, S.S., Alonso-Rodriguez, A., Dai, L., Xu, Q., & Huang, R. 2019: Coseismic landslides triggered by the 2018 Hokkaido, Japan (Mw 6.6), earthquake: spatial distribution, controlling factors, and possible failure mechanism, Landslides, 16, 1551–1566.

P 20.2
Both urbanization and elevation constrict forest greening in the Pearl River Delta, China

Jing Xie

Faculty of Architecture, The University of Hong Kong, Pokfulam, Hong Kong, China (xiej412@hku.hk)

Environmental gradients of build-up areas in urban domains and suburban regions as well as of topography in rural and natural regions can affect and shape the behavior of forest growth in various ways. However, our understanding of the combined impacts of both urbanization and elevation on forest greening based on spatial variation of local climate zone (LCZ) is limited. A more in-depth investigation and evaluation hence is needed.

In this study, we tested the spatial variations and temporal changes of satellite-derived time-series greenness of forested regions, combined with LCZ and digital elevation model (DEM) in subtropical highly urbanized Pearl River Delta region for the period of 2000–2019. Average values and inter-annual trends were analyzed for time-series forest greenness in order to clarify the variation of these spatial and temporal values with distances to patterns from urban centers (LCZ 1: Compact and high-rise) between 0–55,250 meter and with elevation ranging from 0 to 1,556 meter above sea level.

It is found that the average value of peak greenness is lower in urban domains (< 2,000 meters from urban centers) than in suburban (between 2,000–5,000 meters from urban centers) and rural (> 5,000 meters from urban centers). The average value is also lower at high elevations than at low elevations in rural regions. Also, the forest peak greenness in urban domains shows a more slanted inter-annual increasing trend than in suburban and rural regions. Moreover, drastic volatility in inter-annual dynamics are more pronounced at forested areas adjoining compact and high-rise LCZ types than that adjoining open, mid- and lower-rise LCZ types. The effects of built-up LCZ types on forest greenness are stronger in strength and higher in magnitude than effects of elevation in urban and suburban regions. However, the situation is vice-versa in rural regions, with the effects of elevation on forest greening in rural regions are more pronounced than the built-up LCZ types.

We conclude that both urbanization and topography affect forest greening, and these effects are especially pronounced in urban domains and rural high-elevation zones. The results suggest that forest ecosystems adjoining urban centers (i.e. compact and high-rise built-up types) and high elevation above 1,000 meters above sea level are especially sensitive to the variation of environmental factors and projected climate change scenarios in the Pearl River Delta region.